A New Conjugate Gradient Method for Impact Load Identification of Stochastic Composite Structures

Linjun Wang

Hubei Key Laboratory of Hydroelectric Machinery Design and Maintenance, College of Mechanical and Power Engineering, China Three Gorges University, Yichang, Hubei 443002, PR China
School of Chemistry, Physics and Mechanical Engineering, Queensland University of Technology, Brisbane, QLD 4001, Australia

Hongchun Wu

Hubei Key Laboratory of Hydroelectric Machinery Design and Maintenance, College of Mechanical and Power Engineering, China Three Gorges University, Yichang, Hubei 443002, PR China

Youxiang Xie

College of Science Technology, China Three Gorges University, Yichang, Hubei 443002, PR Chin

(Received 4 July 2023; accepted 26 October 2024)

This paper presents a novel conjugate gradient method to identify the impact force of stochastic composite structure. Firstly, the proposed method is established based on constructing a new gradient regularization operator, and its stability and global convergence are strictly proven. Moreover, the proposed method solves the deterministic inverse problem of composite laminated cylindrical shells. Then, using the matrix perturbation method, the uncertain inverse problem of the impact force reconstruction of stochastic structure is converted to definite inverse problems. At last, the statistical properties of the reconstructed impact load are also analyzed. Numerical simulations show that the proposed method performs well in identifying the impact force of composite laminated cylindrical shells with stochastic and non-stochastic properties.

1. INTRODUCTION

Nowadays, in many engineering cases, it is essential to get relevant information about the impact of dynamic load on the design of engineering structures.[1–6] However, the direct measurement of the impact loads on actual engineering structures is not straightforward in some cases, but rather the more easily obtainable structure responses. Therefore, many researchers have researched and developed several practical computation algorithms to obtain the impact force[7–11] in the time domain and frequency domain.

Li et al. proposed a new method for time domain force identification, which can identify the low and high-order dynamic components at the same time with high precision.[12] The time domain method researched the time history and the variation process of the identified load.[13–15] Hou et al. developed a load identification model that can be extended to the problem of moving load identification, which is based on the hpd-s format PIM.[16] Pan et al. proposed a firefly algorithm to obtain moving loads from strain responses, and only one sensor can accurately identify two moving loads.[17] He et al. used composite triangular wavelets to identify dynamic force.[18] Feng et al. proposed an element based on the Bayesian regularization method to deal with the ill-conditioned problem of time-domain load identification.[19] A non-iterative inverse method based on Newmark and Finite Element Method (FEM) was proposed for the identification of the dynamic loads of different structures.[20] Yan et al. proposed a novel approach to identifying the impact position and reconstructing the impact force's time history on composite structures through dynamic strain measurement.[21] A novel time domain load identification method based on Bayesian framework regularization was presented to solve the problem of bad conditioning.[22] Tang et al. presented a new approach for load identification based on stochastic response power spectrum density and proved its correctness in simple beam bridge load analysis.[23,24] A kind of Chebyshev polynomial recognition method, composed of time history and location, is presented.[25]

However, there is much-related research on dynamic load identification, which needs further development. In addition, most of the research above is attributed to the deterministic inverse problem because the geometric and material values are deterministic.[26–28] There are many uncertainties[29] in practical engineering, such as manufacturing errors and the unpredictable environment. Therefore, it is necessary to involve rational modeling and multiple sources of uncertainty in the research of uncertain load identification.[30–33] So, it is very important to do quantitative research on the uncertainty in identifying definite loads.[34,35] Accurate impact load information is essential in the impact dynamics and subsequent safety assessment of practical engineering. Furthermore, the impact load identification of stochastic structures is much more complicated, worthy, and urgent to investigate. Also, less work on stochastic impact load identification has been conducted in recent years. Additionally, in the authors' previous work,[36] it was based on β_k^{WDX} which did not perform well in maintaining significant singular values and filtering small singular values and just only considered deterministic dynamic load identification. Therefore, this paper proposes a modified conjugate gradient (MCG) method to calculate the impact load of composite laminated cylindrical shells with stochastic structure parameters. Statistical characteristics of reconstructed impact force are also evaluated.

The following sections of the paper are organized as follows. In section 2, we introduce the newly developed conjugate gradient method, and demonstrate its stability and global convergence by means of mathematics. Sections 3 and 4 are devoted to the application of the present method to the impact load identification of composite laminated cylindrical shells with multi-source random properties.

2. CONJUGATE GRADIENT METHOD

2.1. Improvement of New Conjugate Gradient Method

In this paper, we consider the following unconstrained optimization problem:

$$\min_{w \in R^n} H(w). \tag{1}$$

The gradient of the continuously differentiable function $H : R^n \to R$ at point w_k is denoted by $g(w_k)$. Its iterative form is given as:

$$w_{k+1} = w_k + \alpha_k d_k, \quad k = 0, 1, 2, \cdots ; \tag{2}$$

where α_k is the step size, and the search direction is d_k. Generally, the step α_k can be obtained based on the Wolfe line search method. Here we define the search direction d_k as follows:

$$d_k = \begin{cases} -g_0, & k = 0 \\ -g_k + \beta_k d_{k-1}, & k \geq 1 \end{cases} ; \tag{3}$$

where β_k is a scalar, and g_k is the gradient of $H(w)$ at the point w_k. Different parameters β_k correspond to different conjugate gradient methods. Many researchers have developed many new different conjugate gradient methods. Based on this, this paper proposes a new conjugate gradient method in which β_k is defined as:

$$\beta_k = \begin{cases} \dfrac{g_k^T (g_k - \mu \frac{d_{k-1} g_k^T}{\|d_{k-1}\|^2} d_{k-1})}{d_{k-1}^T (g_k - g_{k-1})} & g_k^T g_{k-1} \geq 0, \\ \dfrac{g_k^T (g_k + \mu \frac{d_{k-1} g_k^T}{\|d_{k-1}\|^2} d_{k-1})}{d_{k-1}^T (g_k - g_{k-1})} & g_k^T g_{k-1} < 0, \end{cases} ; \tag{4}$$

where $0 < \mu < 1$ is a variable parameter.

The standard Wolf line search is given as:

$$H(w_i + \alpha_k d_k) - H(w_k) \leq \delta \alpha_k g_k^T d_k; \tag{5}$$

$$g(w_k + \alpha_k d_k)^T d_k \geq \sigma g_k^T d_k; \tag{6}$$

where $0 < \delta < \sigma < 1$. Exploiting this line search, the parameter α_k can be obtained. The so-called new conjugate gradient method (MCG) is based on Eqs. (4), (5), (6).

Throughout the paper, we make the following assumptions:
(H1): On the level set $\Omega = \{w \in R^n | H(w_1) \geq H(w)\}$, where w_1 is the initial point, $H(w)$ has a lower-bound value.
(H2): In the neighbouring domain of Ω, the continuously differentiable function $H(w)$ satisfies:

$$\|g(w) - g(y)\| \leq L \|w - y\|, \quad \forall w, y \in \Omega. \tag{7}$$

The computation steps of the proposed method is provided as:
Step 1: $w_1 \in R_n$ is chosen as the initial point, and other parameters are given as: $d_1 = -g_1, \varepsilon > 0, k = 1$. We will stop it when $\varepsilon \geq \|g_1\|$.
Step 2: Exploiting Eq. (5) and Eq. (6), the step length α_k can be computed.
Step 3: According to Eq. (2), w_{k+1} can be obtained. We will stop it when $\|g_{k+1}\| \leq \varepsilon$.
Step 4: According to Eq. (3) and Eq. (4), d_{k+1} and β_k can be obtained.
Step 5: $k = k + 1$; switch to step 2.

2.2. Proof of Global Convergence

Lemma 1 *Let's we assume (H1) and (H2) hold. Based on Eq.* (4)*, exploiting the newly developed conjugate gradient method, we can compute* d_k *and* g_k*. If* $g_k \neq 0$ *for* $k \geq 1$*, then* $g_k^T d_k < 0$.

Proof 1

(1) if $\mu = 0$, then $\beta_k = \beta_k^{DY}$.
(2) if $k = 1$, then $g_1^T d_1 = -\|g_1\|^2 < 0$. The conclusion holds.

Suppose $g_{k-1}^T d_{k-1}$ is negative for $k - 1$ and $k \geq 2$, from Eq. (6) we have:

$$0 < (\sigma - 1) g_{k-1}^T d_{k-1} \leq d_{k-1}^T (g_k - g_{k-1}). \tag{8}$$

Assume that η_k and ξ_k respectively represent the angle between d_{k-1} and g_k, g_{k-1} and g_k vectors, and we have:

$$\cos \eta_k = \frac{g_k^T d_{k-1}}{\|g_k\| \|d_{k-1}\|}, \quad \cos \xi_k = \frac{g_k^T g_{k-1}}{\|g_k\| \|g_{k-1}\|} . \tag{9}$$

If $g_k^T g_{k-1} \geq 0$, employing Eqs. (3), (4) and (6), we have Eq. (10).

If $g_k^T g_{k-1} < 0$, we have Eq. (11)

By mathematical induction, we know that Lemma 1 is true.

Lemma 2 *Under the conditions of (H1) and (H2), when* α_i *is chosen based on Eq.* (5) *and* (6)*, we can obtain:*

$$0 \leq \beta_k \leq \frac{g_k^T d_k}{g_{k-1}^T d_{k-1}}. \tag{12}$$

Proof 2

From Eq. (4) and the angle ξ_k and η_i, we can obtain:

$$\beta_k = \frac{\|g_k\|^2 (1 - \mu \cos \xi_k \cos^2 \eta_k)}{d_{k-1}^T (g_k - g_{k-1})} \geq 0 (g_k^T g_{k-1} \geq 0); \tag{13}$$

$$g_k^T d_k = -\|g_k\|^2 + \beta_k g_k^T d_{k-1} - \|g_k\|^2 = + \frac{g_k^T \left(g_k - \mu \frac{\|g_k\| g_{k-1}}{\|g_{k-1}\|^2} \cdot \frac{(g_k^T d_{k-1})^2}{\|g_k^T\|^2 \|d_{k-1}\|^2} \right)}{d_{k-1}^T (g_k - g_{k-1})} g_k^T d_{k-1}$$
$$= \frac{-\|g_k\|^2 (d_{k-1}^T g_k + d_{k-1}^T g_{k-1} + g_k^T d_{k-1}) - \frac{\mu g_k^T \|g_k\| g_{k-1}}{\|g_{k-1}\|} \cdot \frac{(g_k^T d_{k-1})^2}{\|g_k\|^2 \|d_{k-1}\|^2} g_k^T d_{k-1}}{d_{k-1}^T (g_k - g_{k-1})}$$
$$= \frac{d_{k-1}^T g_{k-1} \|g_k\|^2 - \mu \|g_k\|^2 \cos^2 \eta_k \cos \xi_k \cdot g_k^T d_{k-1}}{(g_k - g_{k-1})^T d_{k-1}} \leq \frac{g_{k-1}^T d_{k-1} \|g_k\|^2 (1 - \mu\sigma \cos \xi_k \cos^2 \eta_k)}{d_{k-1}^T (g_k - g_{k-1})} < 0. \quad (10)$$

$$d_k^T g_k = \beta_k g_k^T d_{k-1} - \|g_k\|^2 = -\|g_k\|^2 + \frac{g_k^T \left(g_k + \mu \frac{\|g_k\| g_{k-1}}{\|g_{k-1}\|^2} \cdot \frac{(g_k^T d_{k-1})^2}{\|g_k^T\|^2 \|d_{k-1}\|^2} \right)}{d_{k-1}^T (g_k - g_{k-1})} g_k^T d_{k-1}$$
$$= \frac{-\|g_k\|^2 d_{k-1}^T g_k + \|g_k\|^2 d_{k-1}^T g_{k-1} + \|g_k\|^2 g_k^T d_{k-1} + \frac{\mu g_k^T \|g_k\| g_{k-1}}{\|g_{k-1}\|} \cdot \frac{(g_k^T d_{k-1})^2}{\|g_k\|^2 \|d_{k-1}\|^2} g_k^T d_{k-1}}{d_{k-1}^T (g_k - g_{k-1})}$$
$$= \frac{\|g_k\|^2 d_{k-1}^T g_{k-1} + \mu \|g_k\|^2 \cos^2 \eta_k \cos \xi_k \cdot g_k^T d_{k-1}}{d_{k-1}^T (g_k - g_{k-1})} \leq \frac{\|g_k\|^2 g_{k-1}^T d_{k-1} (1 + \mu\sigma \cos \xi_k \cos^2 \eta_k)}{d_{k-1}^T (g_k - g_{k-1})} < 0. \quad (11)$$

$$\beta_k = \frac{\|g_k\|^2 (1 + \mu \cos \xi_k \cos^2 \eta_k)}{d_{k-1}^T (g_k - g_{k-1})} \geq 0 (g_k^T g_{k-1} < 0). \quad (14)$$

So, $\beta_k \geq 0$.

Next, we prove that $\beta_k \leq \frac{g_k^T d_k}{g_{k-1}^T d_{k-1}}$.

$$\beta_k = \frac{\|g_k\|^2 (1 - \mu \cos \xi_k \cos^2 \eta_k)}{d_{k-1}^T (g_k - g_{k-1})} \leq \frac{(1 - \sigma\mu \cos \xi_k \cos^2 \eta_k) \|g_k\|^2}{d_{k-1}^T (g_k - g_{k-1})} \leq \frac{g_k^T d_k}{g_{k-1}^T d_{k-1}} (g_k^T g_{k-1} \geq 0); \quad (15)$$

$$\beta_k = \frac{\|g_k\|^2 (1 + \mu \cos \xi_k \cos^2 \eta_k)}{d_{k-1}^T (g_k - g_{k-1})} \leq \frac{\|g_k\|^2 (1 + \sigma\mu \cos \xi_k \cos^2 \eta_k)}{(g_k - g_{k-1}) d_{k-1}^T} \leq \frac{g_k^T d_k}{g_{k-1}^T d_{k-1}} (g_k^T g_{k-1} < 0). \quad (16)$$

In summary, $\beta_k \leq \frac{g_k^T d_k}{g_{k-1}^T d_{k-1}}$. So $0 \leq \beta_k \leq \frac{g_k^T d_k}{g_{k-1}^T d_{k-1}}$, and Lemma 2 holds.

Theorem 1 *Under the conditions of (H1) and (H2), if we consider any iteration of Eq.* (3), *in which α_k follows the standard Wolfe line search conditions and d_k satisfies a descent direction, then we obtain:*

$$\sum_{k \geq 1} \frac{(g_k^T d_k)^2}{\|d_k\|^2} < +\infty. \quad (17)$$

Proof 3

From Lemma 1, we have $g_k^T d_k < 0$. Therefore, the following conclusion holds:

$$0 < (\sigma - 1) g_k^T d_k \leq d_k^T (g_{k+1} - g_k). \quad (18)$$

From (H2), we have:

$$d_k^T (g_{k-1} - g_k) \leq L \alpha_k \|d_k\|^2. \quad (19)$$

Thus, we can obtain:

$$\alpha_k \geq \frac{(\sigma - 1) g_k^T d_k}{L \|d_k\|^2}. \quad (20)$$

Because the sequences H_k are monotonic decreasing and convergent, we get:

$$H_k - H_{k-1} \geq -\delta \alpha_k g_k^T d_k \geq \frac{-\delta(\sigma - 1)({d_k}^T g_k)^2}{\|d_k\|^2 L} = \frac{(1 - \sigma)\delta}{L} \frac{(g_k^T d_k)^2}{\|d_k\|^2}. \quad (21)$$

Taking the limit of the sum of both sides of Eq. (21), we get:

$$\sum_{k \geq 1} \frac{(1 - \sigma)\delta}{L} \frac{({d_k}^T g_k)^2}{\|d_k\|^2} \leq \sum_{k \geq 1} (H_k - H_{k-1}) = H_1 - \lim_{k \to \infty} H_k < +\infty. \quad (22)$$

Therefore, Eq. (17) holds, that is, Theorem 1 is true.

Theorem 2 *Under the conditions of (H1), (H2) and Lemma 1, α_k is chosen according to the standard Wolfe line search conditions. β_k is chosen as Eq.* (4)*. Then we have that:*

$$\lim_{k \to \infty} \inf \|g_k\| = 0. \quad (23)$$

Proof 4

Assume by contradiction that Eq. (23) does not hold. For all k, there exists a constant $\lambda > 0$,

Herein we use the proof by contradiction. Suppose Eq. (23) is not satisfied, i.e., there must be a positive parameter λ such that:

$$\|g_k\| \geq \lambda. \tag{24}$$

Squaring both sides of $d_k = -g_k + \beta_k d_{k-1}$, we obtain that:

$$\beta_k^2 \|d_{k-1}\|^2 - \|g_k\|^2 - 2g_k^T d_k = \|d_k\|^2. \tag{25}$$

Dividing the above formula by $(g_k^T d_k)^2$, yields:

$$\begin{aligned}\frac{\|d_k\|^2}{(d_k^T g_k)^2} &= \frac{\beta_k^2 \|d_{k-1}\|^2}{(g_k^T d_k)^2} - \frac{2}{g_k^T d_k} - \frac{\|g_k\|^2}{(g_k^T d_k)^2} \\ &= \frac{\beta_k^2 \|d_{k-1}\|^2}{(g_k^T d_k)^2} + \frac{1}{\|g_k\|^2} - (\frac{1}{\|g_k\|} + \frac{\|g_k\|}{g_k^T d_k})^2 \\ &\leq \frac{\beta_k^2 \|d_{k-1}\|^2}{(g_k^T d_k)^2} + \frac{1}{\|g_k\|^2}.\end{aligned} \tag{26}$$

From Eq. (12) of Lemma 2, we have:

$$\begin{aligned}&\frac{\|d_k\|^2}{(g_k^T d_k)^2} \leq \frac{1}{\|g_k\|^2} + \frac{\|d_{k-1}\|^2}{(g_k^T d_k)^2} \frac{(g_k^T d_k)^2}{(g_{k-1}^T d_{k-1})^2} = \\ &\frac{\|d_{k-1}\|^2}{(g_{k-1}^T d_{k-1})^2} + \frac{1}{\|g_k\|^2}.\end{aligned} \tag{27}$$

From Eq. (3), we can get:

$$d_1 = -g_1. \tag{28}$$

Thus, we have:

$$\frac{\|d_1\|^2}{(g_1^T d_1)^2} = \frac{1}{\|g_1\|^2}. \tag{29}$$

By recursion, we obtain:

$$\frac{\|d_k\|^2}{(g_k^T d_k)^2} \leq \sum_{j=1}^{k} \frac{1}{\|g_j\|^2} \leq \frac{k}{\lambda^2}. \tag{30}$$

That is:

$$\frac{(g_k^T d_k)^2}{\|d_k\|^2} \geq \frac{\lambda^2}{k}. \tag{31}$$

Summing both sides of Eq. (31), we get:

$$\sum_{k\geq 1} \frac{(g_k^T d_k)^2}{\|d_k\|^2} \geq \lambda^2 \sum_{k \geq 1} \frac{1}{k} = +\infty. \tag{32}$$

This contradicts Eq. (17). So, Theorem 2 holds.

3. IMPACT FORCE RECONSTRUCTION WITHOUT CONSIDERING STOCHASTIC FACTORS

Next, we will apply the newly developed MCG method to the impact load identification of a composite structure.

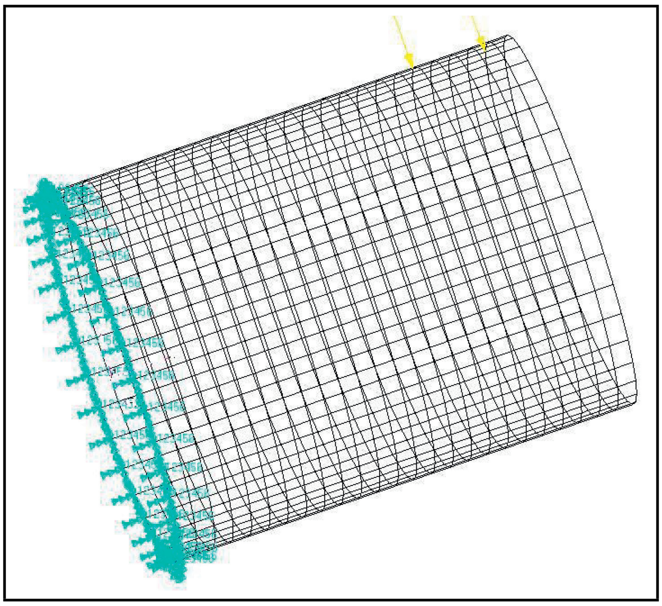

Figure 1. Composite laminated

Under the assumption of time invariance and linearity, the impact load of the structure can be calculated indirectly. The corresponding reaction of an engineering structure at an arbitrary point can be computed according to the following formula:[30,32,35,37]

$$y(t) = \int_0^t p(\tau) g(t-\tau) d\tau; \tag{33}$$

in which $g(t), y(t)$ and $p(\tau)$ represent the Green's function, the displacement response, and the expected known load, respectively.

In this paper, a composite laminated cylindrical shell[36,38] is selected as the research object to verify the effectiveness and stability of the proposed method. Figure 1 shows the finite element model (FEM) of the composite laminated cylindrical shell. It has 936 nodes and 900 grids. The cylindrical shell size is 200.0 mm in middle radius, 10.0 mm in thickness, and 500.0 mm in length. It consists of one carbon/epoxy layer and one glass/epoxy layer. Its stacking sequence is denoted by $[C90/G+45/G-45]_s$, where C and G stand for the carbon/epoxy and the glass/epoxy layer, respectively, and $90, +45$, and -45 stand for the angle of fiber-orientation to the center axis. The subscript s means that it is symmetrically stacked. The corresponding specific parameter information such as material properties can be referred to Wang, Gao, Xie, Fu, Du;[36] Wang and Xie.[38] The actual impact force is given as:

$$\begin{aligned} F_1(t) &= \begin{cases} 0, & t \in [0, t_d/4] \\ q_1 \sin(\frac{2\pi t}{5t_d}), & t \in (t_d/4, t_d/2] \\ 0, & t \in (t_d/2, 3t_d/4] \\ q_2 \sin(\frac{2\pi t}{5t_d}), & t \in (3t_d/4, t_d] \\ 0, & t \in (t_d, 5t_d/4] \end{cases} ; \\ F_2(t) &= \frac{2q_1 t}{t_d} e^{-200t}, \quad t \in [0, 5t_d/4] \end{aligned} \tag{34}$$

where $t_d = 0.04$ s, $q_1 = -1000$ N, $q_2 = -500$ N. Using FEM, we get the radial displacement response. In order to simulate the real environment, we increased the noise level by 5% to

Table 1. The identified impact force at five time points at 5% noise level.

			Tikhonov method		MCG method		FRCG method	
	Time point	Real force	Identified force	Error (%)	Identified force	Error (%)	Identified force	Error (%)
F_1	0.005	0	1.17	0.12	-57.00	5.70	-18.36	1.84
F_2	0.002	670.32	684.19	1.51	675.14	0.52	714.14	4.76
F_1	0.015	1000	1064.59	6.46	1024.5	2.45	933.50	6.65
F_2	0.005	919.70	949.49	3.24	936.19	1.79	906.30	1.46
F_1	0.033	404.51	359.37	4.51	350.57	5.39	388.83	1.57
F_2	0.012	544.31	509.92	3.74	536.5	0.85	582.03	4.10
F_1	0.035	500	466.50	3.35	471.48	2.85	475.98	2.40
F_2	0.025	84.22	98.71	1.58	92.82	0.93	80.96	0.35
F_1	0.038	293.89	310.68	1.68	265.24	2.86	313.71	1.98
F_2	0.035	15.96	-18.11	3.70	4.92	1.20	41.30	2.76
Error (%)			Maximum	Average	Maximum	Average	Maximum	Average
F_1			10.64	3.36	10.68	3.07	10.87	3.09
F_2			8.10	2.41	8.54	2.35	8.29	2.42

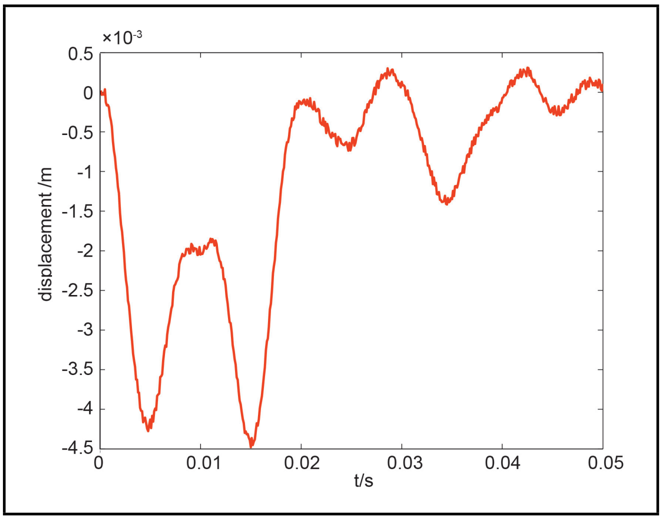

Figure 2. The radial displacement response at one point.

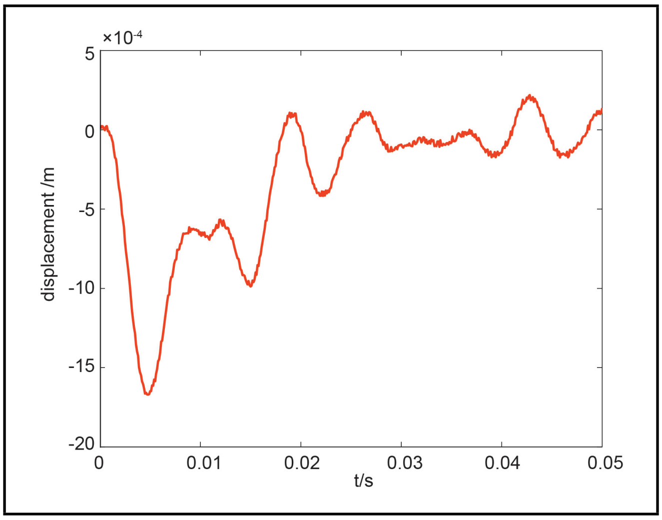

Figure 3. The radial displacement response at the other point.

get data close to the practical measurement results. The corresponding displacement responses are shown in Figures 2 and 3. The convergence control error and the parameter of the gradient regularization operator are given as $\varepsilon = 0.11$ and $\mu = 0.6$, respectively. The traditional Tikhonov regularization method, MCG, and the original conjugate gradient method (FRCG) are evaluated with the average and relative estimation errors, and their calculation formulas are respectively given as:

$$F_{\text{Average}} = \frac{1}{n}\sum_{i=1}^{n}\left|\frac{F_{\text{Identified}}(i) - F_{\text{Real}}(i)}{\max\{F_{\text{j}}\}}\right| * 100;$$

$$\tilde{F} = \left|\frac{F_{\text{Identified}}(i) - F_{\text{Real}}(i)}{\max\{F_{\text{j}}\}}\right| * 100;$$

in which $i = 1, 2, \cdots, n$, $j = 1, 2$.

It can be seen from Figures 4 to 7 that three regularization methods, such as Tikhonov, MCG, and FRCG, can identify the impact force well. Figures 4 and 5 show that the MCG method is better than the conventional Tikhonov regularization method and FRCG at 5% noise level. At the same time, according to the specific calculation results in Figures 6, 7, and Table 1, the most relative error of Tikhonov and FRCG is greater than that of MCG. The maximum identification error of Tikhonov and FRCG in reconstructing F_1 is 10.64%, 10.87%, and the maximum error of the MCG method is 10.68%. The average error

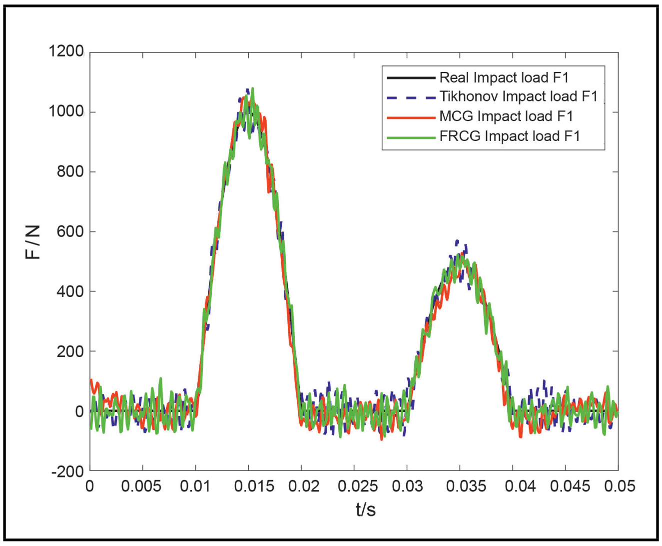

Figure 4. The reconstructed F_1.

rate of the traditional Tikhonov regularization method, MCG, and FRCG is 3.36%, 3.07%, and 3.09%, $respectively$. For impact load F_2, the maximum identification error of Tikhonov and MCG is respectively 8.1%, 8.54%, and FRCG's is 8.29%. Additionally, the average identification error of Tikhonov is 2.41%, and the average error of the MCG and FRCG methods

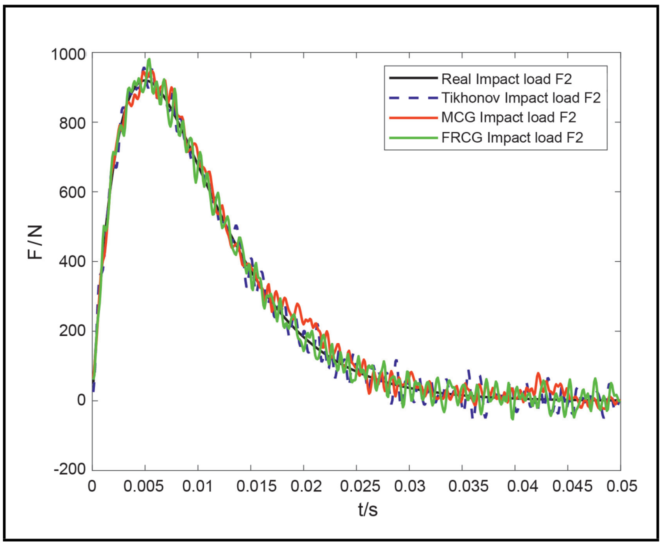

Figure 5. The reconstructed F_2.

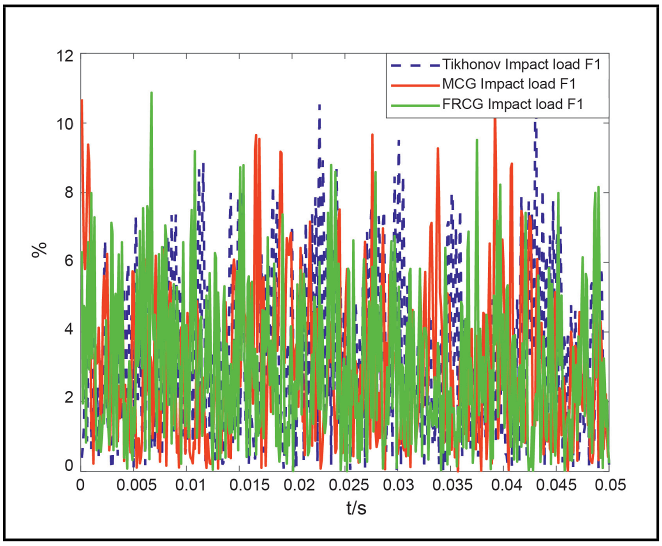

Figure 6. The relative error for F_1.

is $2.35\% and 2.42\%$. The above research results show that the MCG algorithm performs well in impact force reconstruction without considering stochastic factors and verify the stability and effectiveness of the proposed method.

4. IMPACT LOAD IDENTIFICATION CONSIDERING STOCHASTIC FACTORS

4.1. Problem Formulation

Green's function is random to a certain extent when we consider the practical engineering case that the geometrical and physical parameters of the structure are partly random. Thus, the expected known impact load and the Green function are stochastic and related to time and random structure parameters. On this basis, the convolution integral formula used to identify the impact load of random structures is derived as:

$$\int_0^t p(\tau,\xi)g(t-\tau,\xi)d\tau = y(t); \tag{35}$$

where ξ is a stochastic structure parameter.

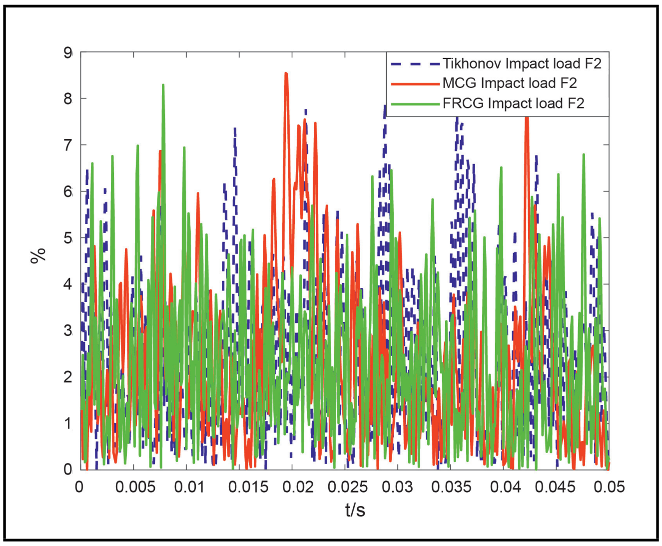

Figure 7. The relative error for F_2.

The time history is split into Q equal intervals and Δt represents each interval. Then at $t = h\Delta t$ $(h = 0, 1, \cdots, Q)$, we have Eqs. (36) and (37) in which the Green's function and the response are denoted by $g(t_h, \xi)$ and $y(t_h)$, respectively, and $p(t_h, \xi)$ considers the unknown load.

Then, we use the simplified Eq. (37) to investigate the impact force identification with random factors.

4.2. Perturbation Analysis

Regarding the accuracy of the results, the Monte Carlo method is considered the best method to solve the inverse problem Eq. (37) and is often used to check the accuracy of other methods. However, its computation cost is much higher because of many matrix calculations. The perturbation technology is usually exploited to transform the impact force identification with uncertain factors into deterministic impact load identification.

Among them, the Taylor expansion method is employed to describe the random parameters:

$$\xi{=}\Delta\xi_{\mathrm{r}} + \xi_{\mathrm{d}}; \tag{38}$$

$$\xi_l{=}\Delta\xi_{\mathrm{rl}} + \xi_{\mathrm{dl}}; \tag{39}$$

in which $\xi = (\xi_1, \xi_2, \cdots, \xi_q)$.

Here, d and r denote the mean and fluctuation of stochastic parameters, respectively. Thus, we obtain:

$$G(\xi) = G_d + \Delta G_r; \tag{40}$$

$$p(\xi) = \Delta p_r + p_d. \tag{41}$$

Substituting Eq. (40) and Eq. (41) into Eq. (37), we obtain:

$$y = (G_d + \Delta G_r)(p_d + \Delta p_r). \tag{42}$$

Expanding Eq. (42), yields:

$$y = G_d p_d; \tag{43}$$

$$-\Delta G_r p_d = \Delta p_r G_d. \tag{44}$$

$$\begin{pmatrix} g(t_1,\xi) & 0 & \cdots & 0 \\ g(t_2,\xi) & g(t_1,\xi) & \cdots & 0 \\ \vdots & \vdots & \ddots & \vdots \\ g(t_Q,\xi) & g(t_{Q-1},\xi) & \cdots & g(t_1,\xi) \end{pmatrix} \begin{pmatrix} p(t_0,\xi) \\ p(t_1,\xi) \\ \vdots \\ p(t_{Q-1},\xi) \end{pmatrix} \Delta t = \begin{pmatrix} y(t_1) \\ y(t_2) \\ \vdots \\ y(t_Q) \end{pmatrix}; \tag{36}$$

i.e.

$$y = G(\xi)P(\xi). \tag{37}$$

Noticing the certainty of y and G_d in Eq. (43), we can get the mean of the load using the conventional regularization method. We can obtain Δp_r from Eq. (44).

Aditionally, considering that $\Delta\xi_{rl}$ is infinitesimal[30,32] compared to ξ_{dl}, we can obtain:

$$\Delta G_r \approx \sum_{l=1}^{q} G_{d,l}\Delta\xi_{rl}; \tag{45}$$

$$\Delta p_r \approx \sum_{l=1}^{q} p_{d,l}\Delta\xi_{rl}; \tag{46}$$

in which the equivalent derivative of ξ_l is denoted by d, l.

Then we can get:

$$-G_{d,l}p_d = G_d p_{d,l}. \tag{47}$$

Thus, for $l = 1, 2, \cdots, q$, we have:

$$y = G_d p_d; \tag{48a}$$

$$G_d p_{d,l} = -G_{d,l}p_d; \tag{48b}$$

Actually, Eq. (48a) and (48b) can be treated similarly. Moreover, the sensitivity $G_{d,l}$ in Eq. (48b) can be numerically computed.

Taking into account the practical engineering case, we can re-express Eq. (48a) as:

$$y_{err} = G_d p_{tr}; \tag{49}$$

where y_{err} is a measured response containing the noise.

4.3. Analysis of the Statistical Feature

In this section, the lower boundary, the upper boundary, and statistical characteristics will be investigated.

Using Eq. (41), we can obtain that:

$$p_d = \mathrm{E}(\triangle p_r) + \mathrm{E}(p_d) = \mathrm{E}(p(\xi)). \tag{50}$$

We have:

$$\begin{aligned} \mathrm{var}(p(\xi)) &= \int_{-\infty}^{\infty} \cdots \int_{-\infty}^{\infty} f(\xi)(E(p(\xi)) - p(\xi))^2 d\xi \\ &\approx \int_{-\infty}^{\infty} \cdots | \int_{-\infty}^{\infty} (\sum_{l=1}^{q} \Delta\xi_{rl}p_{d,l})^2 f(\xi)d\xi \\ &= \sum_{i=1}^{q}\sum_{j=1}^{q} p_{d,i}p_{d,j}\mathrm{cov}(\xi_i,\xi_j) \end{aligned}; \tag{51}$$

$$\mathrm{cov}(\xi_i,\xi_j) = \int_{-\infty}^{\infty} \cdots \int_{-\infty}^{\infty} \Delta\xi_{ri}\Delta\xi_{rj}f(\xi)d\xi = \rho_{ij}\sigma(\xi_i)\sigma(\xi_j). \tag{52}$$

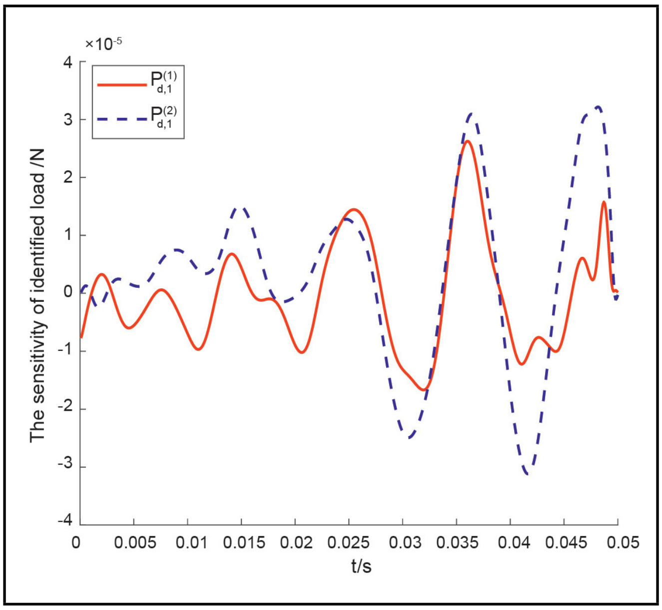

Figure 8. The sensitivity of impact force about ξ_1.

Specifically, if there is no correlation between ξ_i and ξ_j, we have:

$$\mathrm{var}(p(\xi)) = \sum_{i=1}^{q} (p_{d,i}\sigma(\xi_i))^2. \tag{53}$$

Then, we can get the upper and lower bounds of the determined collision load as:

$$\begin{cases} p_{up} = p_d + [4\,\mathrm{var}(p(\xi))]^{\frac{1}{2}} \\ p_{down} = p_d - [4\,\mathrm{var}(p(\xi))]^{\frac{1}{2}} \end{cases}. \tag{54}$$

Furthermore, the mean change factor of the nth reconstructed force is given by:

$$CV(p^{(n)}(\xi)) = \frac{\sum_{k=0}^{Q-1}\sqrt{\mathrm{var}(p^{(n)}(t_k,\xi))}}{\sum_{k=0}^{Q-1}E(p^{(n)}(t_k,\xi))} \times 100\%. \tag{55}$$

4.4. Engineering Application

We again investigate the engineering problem of Section 3. Because of the discontinuity of materials, Young's modulus ξ_1 of glass/epoxy resin and ξ_2 of carbon/epoxy resin are independent normal variables. The corresponding mathematical expectations are $mu_1 = 38490000$ kPa and $mu_2 = 142170000$ kPa, respectively. Additionally, their variation coefficients are set as $CV_i = 5\%(i = 1, 2)$. Herein, we consider the noise level as 5%.

When the random variables ξ_1 and ξ_2 take their average values, respectively, using Eq. (48b), the sensitivity of p_1 and p_2 to random variables ξ_1 and ξ_2 can be respectively obtained.

Table 2. The detailed identification.

F1				F2			
Time point	True load (N)	Reconstructed load (N)	Error (%)	Time point	True load (N)	Reconstructed load (N)	Error (%)
0.005	0	138.69	13.87	0.002	670.32	690.99	2.25
		8.55	0.86			654.8	1.69
0.015	1000	1042.1	4.21	0.005	919.70	954.52	3.79
		1005.2	0.52			879.96	4.32
0.033	404.51	462.68	5.82	0.012	544.31	550.84	0.71
		352.33	5.22			516.49	3.02
0.035	500	518.53	1.85	0.025	84.22	192.41	11.76
		349.82	15.02			24.89	6.45
0.038	293.89	153.7	14.02	0.035	15.96	160.61	15.73
		74.84	21.91			10.94	0.5

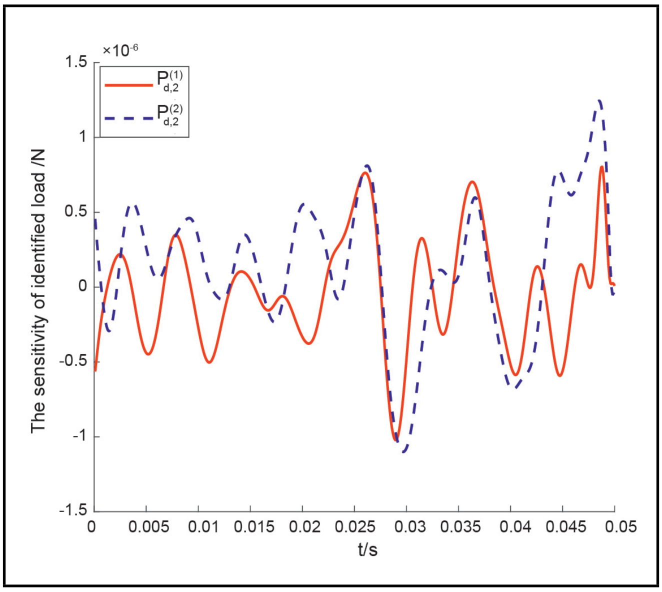

Figure 9. The sensitivity of impact force about ξ_2.

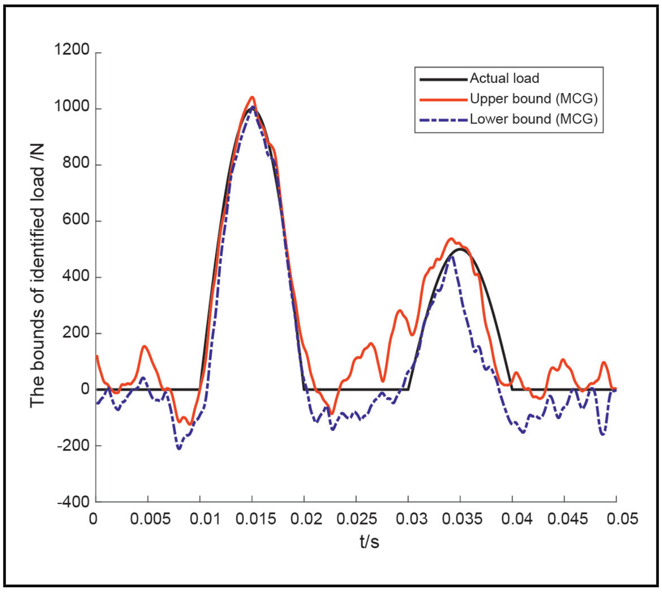

Figure 10. The bound of identified F_1.

They are shown in Figures 8 and 9. Figures 10 and 11 show the upper and lower limits of the reconstructed impact force by the proposed algorithm.

As can be seen from Figures 10 and 11, most of the actual impact load is between the conveyor belt, i.e., between the lower and upper boundaries. It is found that MCG and the matrix perturbation method can get the lower and upper boundaries of impact load well in the presence of noise interference. In addition, because random structural parameters significantly affect the identification accuracy, the boundary width is relatively large at the two collision load peaks. Table 2 shows specific results at five time points, such as the lower and upper deviation of the identified impact load.

The results in Table 2 show that the maximum error between boundary load and real load is 21.91%. In the reconstruction of the first impact force, the maximum boundary error value is 21.91%, the minimum boundary deviation value is 0.52%, and the coefficient of variation is 12.91%. In the reconstruction of the second impact force, the maximum boundary error value is 15.73%, the minimum boundary deviation value is 0.55%, and the coefficient of variation is 12.85%. Based on the above analysis, we find that the identification of the impact load of stochastic structure is affected by the influence of random structural parameters.

5. CONCLUSION

This paper proposes a new conjugate gradient method for impact force identification with and without considering random structural parameters. Considering that the structure parameters are random in practical engineering, we construct the uncertain impact load identification model with random characteristics. Exploiting the matrix perturbation method, we transform this model into a deterministic inverse problem, which can be dealt with by the newly developed conjugate gradient method. The present algorithm provides a regularized solution to the deterministic force identification problem. Furthermore, the statistical features of the reconstructed impact force are investigated. Numerical simulations verify that the proposed method is stable and efficient in identifying the impact force. Our method will be exploited in future studies to impact load reconstruction of other composite structures with multi-source stochastic properties. In addition, we plan to apply the proposed method to the inverse problem of dynamic structural reliability.

DECLARATION OF COMPETING INTEREST

The authors declare that they have no known competing financial interests or personal relationships that could have appeared to influence the work reported in this paper.

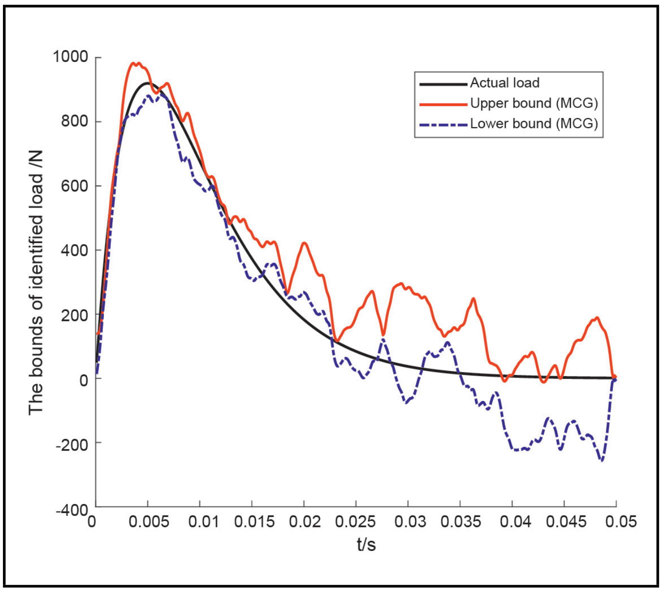

Figure 11. The bound of identified F_2.

ACKNOWLEDGEMENT

This work is supported by the National Natural Science Foundation of China (11202116).

REFERENCES

[1] Lin, J.H., Guo, X.L., and Zhi, H. Computer simulation of structural random loading identification, *Computers and Structures*, **79**(4), 375–387, (2001). https://doi.org/10.1016/S0045-7949(00)00154-1

[2] Zhu, S.Y., and Zhu, L.W. Dynamic load identification on launch vehicle, *Journal of Vibration Engineering and Technologies*, **21**(2), 130–135, (2008). https://doi.org/10.16385/j.cnki.issn.1004-4523.2008.02.011

[3] Martini, D., Hochard, C., and Charles, J.P. Load identification for full-field reconstruction: applications to plates under tension loads, *International Journal for Numerical Methods in Engineering*, **91**(10), 1073–1086, (2012). https://doi.org/10.1002/nme.4304

[4] Jiang, J.H., Ding, M., and Li, J. A novel time-domain dynamic load identification numerical algorithm for continuous systems, *Mechanical Systems and Signal Processing*, **160**, 107881, (2021). https://doi.org/10.1016/j.ymssp.2021.107881

[5] Jiang, J.H., Luo, S.Y., and Zhang, F. One novel dynamical calibration method to identify two-dimensional distributed load, *Journal of Sound and Vibration*, **515**, 116465, (2021). https://doi.org/10.1016/j.jsv.2021.116465

[6] Liu, Y.R., and Wang, L. A robust-based configuration design method of piezoelectric materials for mechanical load identification considering structural vibration suppression, *Computer Methods in Applied Mechanics and Engineering*, **410**, 115998, (2023). https://doi.org/10.1016/j.cma.2023.115998

[7] Mao, B.Y., Xie, S.L., Xu, M.L. Zhang, X.N., and Zhang, G.H. Simulated and experimental studies on identification of impact load with the transient statistical energy analysis method, *Mechanical Systems and Signal Processing*, **46**(2), 307–324, (2014). https://doi.org/10.1016/j.ymssp.2014.01.015

[8] Jang, T.S., Baek, H., Han, S.L., and Kinoshita, T. Indirect measurement of the impulsive load to a nonlinear system from dynamic response: inverse problem formulation, *Mechanical Systems and Signal Processing*, **24**(6), 1665–1681, (2010). https://doi.org/10.1016/j.ymssp.2010.01.003

[9] Hu, N., Matsumoto, S., Nishi, R., and Fukunaga, H. Identification of impact forces on composite structures using an inverse approach, *Structural Engineering and Mechanics*, **27**(4), 409–424, (2007). https://doi.org/10.12989/sem.2007.27.4.409

[10] Liu, Y.R., and Wang, L. Multiobjective-clustering-based optimal heterogeneous sensor placement method for thermo-mechanical load identification, *International Journal of Mechanical Sciences*, **253**, 108369, (2023). https://doi.org/10.1016/j.ijmecsci.2023.108369

[11] Liu, J., Meng, X.H., Zhang, D.Q., Jiang, C., and Han, X. An efficient method to reduce ill-posedness for structural dynamic load identification. *Mechanical Systems and Signal Processing*, **95**, 273–285, (2017). https://doi.org/10.1016/j.ymssp.2017.03.039

[12] Li, Q., and Lu, Q. A revised time domain force identification method based on Bayesian formulation, *International Journal for Numerical Methods in Engineering*, **118**, 411–431, (2019). https://doi.org/10.1002/nme.6019

[13] Law, S.S., Bu, J.Q., and Zhu, X.Q. Time-varying wind load identification from structural responses, *Engineering Structures*, **27**, 1586–1598, (2005). https://doi.org/10.1016/j.engstruct.2005.05.007

[14] Law, S.S., Chan, T.H.T., and Zeng, Q.H. Moving force identification: a time domain method, *Journal of Sound and Vibration*, **201**(1), 1–22, (1997). https://doi.org/10.1006/jsvi.1996.0774

[15] Yi, L., and Shepard, W.S. Dynamic force identification based on enhanced least squares and total least squares schemes in the frequency domain, *Journal of Sound and Vibration*, **282**, 37–60, (2005). https://doi.org/10.1016/j.jsv.2004.02.041

[16] Hou, X.H., Deng, Z.C., and Huang, L.X. Dynamic moving load identification for bridge structures based on precise integration method, *Shock and Vibration*, **26**(9), 142–145+154, (2007). https://doi.org/10.13465/j.cnki.jvs.2007.09.027

[17] Pan, C., and Yu, L. Moving force identification based on firefly algorithm, *Advanced Materials Research* **919-921**, 329–333, (2014). https://doi.org/10.4028/www.scientific.net/AMR.919-921.329

[18] He, W.Y., Wang, Y., and Ren, W.X. Dynamic force identification based on composite trigonometric wavelet shape function, *Mechanical Systems and Signal Processing*, **141**, 106493, (2020). https://doi.org/10.1016/j.ymssp.2019.106493

[19] Feng, W., Li, Q., Lu, Q., Li, C., and Wang, B. Element-wise Bayesian regularization for fast and adaptive force reconstruction, *Journal of Sound and Vibration*, **490**, 115713, (2021). https://doi.org/10.1016/j.jsv.2020.115713

[20] Yu, B., Wu, Y., Hu, P.M., Ding, J.F., Zhou, H.L., and Wang, B.Z. A non-iterative identification method of dynamic loads for different structures, *Journal of Sound and Vibration*, **483**, 115508, (2020). https://doi.org/10.1016/j.jsv.2020.115508

[21] Gang, Y., Hao, S., and Büyükztürk, O. Impact load identification for composite structures using Bayesian regularization and unscented Kalman filter, *Structural Control and Health Monitoring*, **24**(5), (2017). https://doi.org/10.1002/stc.1910

[22] Li, Q.F., and Lu, Q.H. A revised time domain force identification method based on Bayesian formulation, *International Journal for Numerical Methods in Engineering*, **118**, 411–431, (2019). https://doi.org/10.1002/nme.6019

[23] Tang, Q.Z., Xin, J.Z., Jiang, Y., Zhou, J.T., Li, S.J., and Chen, Z.Y. Novel identification technique of moving loads using the random response power spectral density and deep transfer learning, *Measurement*, **195**, 111120, (2022). https://doi.org/10.1016/j.measurement.2022.111120

[24] Zheng, Z.D., Lu, Z.R., Chen, W.H., and Liu, J.K. Structural damage identification based on power spectral density sensitivity analysis of dynamic responses, *Computers and Structures*, **146**, 176–184, (2015). https://doi.org/10.1016/j.compstruc.2014.10.011

[25] Hu, N., Fukunaga, H., Matsumoto, S., Yan, B., and Peng, X.H. An efficient approach for identifying impact force using embedded piezoelectric sensors, *International Journal of Impact Engineering*, **34**, 1258–1271, (2007). https://doi.org/10.1016/j.ijimpeng.2006.05.004

[26] McCann, M.T., Jin, K.H., and Unser, M. Convolutional Neural Networks for Inverse Problems in Imaging: A Review. *IEEE Signal Processing Magazine*, **34**(6), 85–95, (2017). https://doi.org/10.1109/MSP.2017.2739299

[27] Tuan, N.H., Le, D.L., and Nguyen, V.T. Regularized solution of an inverse source problem for a time fractional diffusion equation, *Applied Mathematical Modelling*, **40**, 8244–8264, (2016). https://doi.org/10.1016/j.apm.2016.04.009

[28] Yang, H.J., Jiang, J.H., Chen, G.P., and Zhao, J.M. Dynamic load identification based on deep convolution neural network. *Mechanical Systems and Signal Processing* **185**, 109757, (2023). https://doi.org/10.1016/j.ymssp.2022.109757

[29] Li, Z.S., Wang, L., and Lv, T.Q. A level set driven concurrent reliability-based topology optimization (LS-CRBTO) strategy considering hybrid uncertainty inputs and damage defects updating. *Computer Methods in Applied Mechanics and Engineering*, **405**, 115872, (2023). https://doi.org/10.1016/j.cma.2022.115872

[30] Wang, L.J., Peng, Y.L., Xie, Y.X., Chen, B.J., and Du, Y.X. A new iteration regularization method for dynamic load identification of stochastic structures, *Mechanical Systems and Signal Processing*, **156**, 107586, (2021). https://doi.org/10.1016/j.ymssp.2020.107586

[31] Liu, Y., Wang, L., and Gu, K. A support vector regression (SVR)-based method for dynamic load identification using heterogeneous responses under interval uncertainties, *Applied Soft Computing*, **110**, 107599, (2021). https://doi.org/10.1016/j.asoc.2021.107599

[32] Liu, J., Sun, X.S., Han, X., Jiang, C., and Yu, D.J. Dynamic load identification for stochastic structures based on Gegenbauer polynomial approximation and regularization method, *Mechanical Systems and Signal Processing*, **56–57**, 35–54, (2015). https://doi.org/10.1016/j.ymssp.2014.10.008

[33] Liu, Y.R., Wang, L., Li, M., and Wu, Z.M. A distributed dynamic load identification method based on the hierarchical-clustering-oriented radial basis function framework using acceleration signals under convex-fuzzy hybrid uncertainties, *Mechanical Systems and Signal Processing*, **172**, 108935, (2022). https://doi.org/10.1016/j.ymssp.2022.108935

[34] Liu, J., Cao, L.X., Jiang, C., Ni, B.Y., and Zhang, D.Q. Parallelotope-formed evidence theory model for quantifying uncertainties with correlation, *Applied Mathematical Modelling*, **77**, 32–48, (2020). https://doi.org/10.1016/j.apm.2019.07.017

[35] Liu, J. and Li, K. Sparse identification of time-space coupled distributed dynamic load, *Mechanical Systems and Signal Processing*, **148**, 107177, (2021). https://doi.org/10.1016/j.ymssp.2020.107177

[36] Wang, L.J., Gao, X., Xie, Y.X., Fu, J.J., and Du, Y.X. A New Conjugate Gradient Method and Application to Dynamic Load Identification Problems, *International Journal of Acoustics and Vibration*, **26**, 121–130, (2021). https://doi.org/10.20855/ijav.2021.26.21746

[37] Wang, L.J., Liu, Y., Xie, Y.X., and Chen, B.J. Impact load identification of composite laminated cylindrical shell with stochastic characteristic, *Archive of Applied Mechanics*, **92**, 1397–1411, (2022). https://doi.org/10.1007/s00419-022-02116-2

[38] Wang, L.J., Xie, Y.X. A novel regularization method and application to load identification of composite laminated cylindrical shell, *Journal of Applied Analysis and Computation*, **5**, 570–580, (2015). https://doi.org/10.11948/2015044